ACS OMEGA

Open Access

http://pubs.acs.org/journal/acsodf

Article

Enhanced Ear Cartilage Regeneration with Dual-Network LT-GelMA/F127DA Hydrogel Featuring Nanomicelle Integration

Bingzhang Liu, Yuhan Jiang, Yufeng Tian, Tian Li,* and Duo Zhang*

Cite This: *ACS Omega* 2025, 10, 13570−13582

Read Online

ACCESS | Metrics & More | Article Recommendations | Supporting Information

ABSTRACT: Tissue-engineered cartilage, supported by advancements in photo-cross-linkable hydrogels, offers a promising solution for the repair and regeneration of damaged cartilage in anatomically complex and mechanically demanding sites. Low-temperature soluble GelMA (LT-GelMA) remains in a liquid state at room temperature, allowing for easier handling; however, it has limitations in mechanical strength and structural stability. To address these limitations, we developed a novel dual-network hydrogel combining LT-GelMA with Pluronic F127-diacrylate (F127DA). The resulting hydrogel uniquely integrates the low-temperature solubility of LT-GelMA with the enhanced mechanical strength provided by photo-cross-linkable F127DA nanomicelles. Additionally, the hydrogel exhibits controlled swelling and biodegradation rates. In vitro studies revealed a significant increase in chondrocyte viability by day 7 in formulations with higher F127DA concentrations. In vivo, the hydrogel demonstrated superior neo-cartilage formation in a subcutaneous nude mouse model, as indicated by increased deposition of cartilage-specific extracellular matrix components at 4 and 8 weeks. In summary, we developed a hydrogel with fluidity at room temperature and enhanced mechanical performance. These results indicate that the LT-GelMA/F127DA hydrogel effectively addresses the current gaps in cartilage tissue engineering. The hydrogel's superior performance, especially in promoting cartilage regeneration, positions it as a promising alternative for reconstructive surgery, representing a significant improvement over existing cartilage repair strategies.

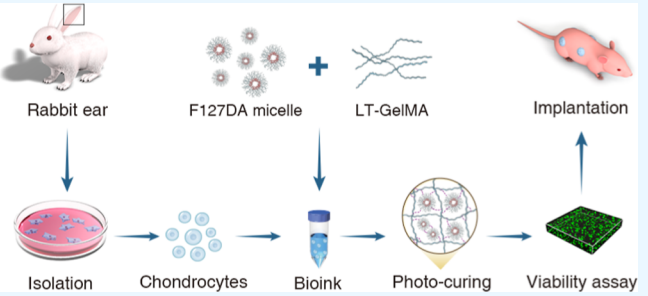

1. INTRODUCTION

Tissue-engineered cartilage has emerged as a promising solution for the repair and regeneration of damaged cartilage in various anatomical sites, including the ear, nose, trachea, and joints.[1−3] These organs and tissues often require the maintenance of specific shapes or the ability to bear mechanical loads, making the enhancement of mechanical properties a critical factor for successful cartilage engineering.[4,5] Achieving adequate mechanical performance in tissue-engineered cartilage involves addressing several challenges, such as replicating the intricate extracellular matrix (ECM) structure, promoting robust cell-matrix interactions, and ensuring long-term durability under physiological stress.[6] Various strategies have been explored to enhance the mechanical properties of engineered cartilage, including optimization of scaffold composition, application of cross-linking techniques, and incorporation of bioactive factors or reinforcement materials.[7−9] These approaches aim to create biomimetic constructs capable of meeting both the functional and structural demands of target tissues.[10,11]

Innovations in biomaterials have facilitated the development of hydrogels that effectively mimic the ECM, providing scaffolds for cell attachment and proliferation.[12,13] Notably, the introduction of photo-cross-linkable hydrogels, such as gelatin methacryloyl (GelMA), represents a pivotal advancement in this field.[14,15] These hydrogels exhibit favorable biocompatibility, which is essential for supporting the chondrogenesis of cartilage cells.[16,17] Moreover, their shape and size can be precisely tailored using techniques such as 3D bioprinting, aligning closely with the complex anatomical requirements of cartilage reconstruction.[18,19] These advancements not only reduce the need for multiple invasive surgeries but also enhance the predictability of outcomes by providing consistent material properties and reliable biological integration, both of which are critical for the successful regeneration of functional cartilage.[20,21]

Low-temperature soluble GelMA (LT-GelMA), synthesized from cold-water fish skin-derived gelatin, has been developed as a promising natural hydrogel material for tissue engineering.[22] Similar to traditional GelMA, LT-GelMA exhibits excellent biocompatibility and effectively supports cell adhesion, proliferation, and differentiation.[23] However, LT-

Received: January 16, 2025
Revised: February 28, 2025
Accepted: March 19, 2025
Published: March 27, 2025

https://doi.org/10.1021/acsomega.5c00476
ACS Omega 2025, 10, 13570−13582

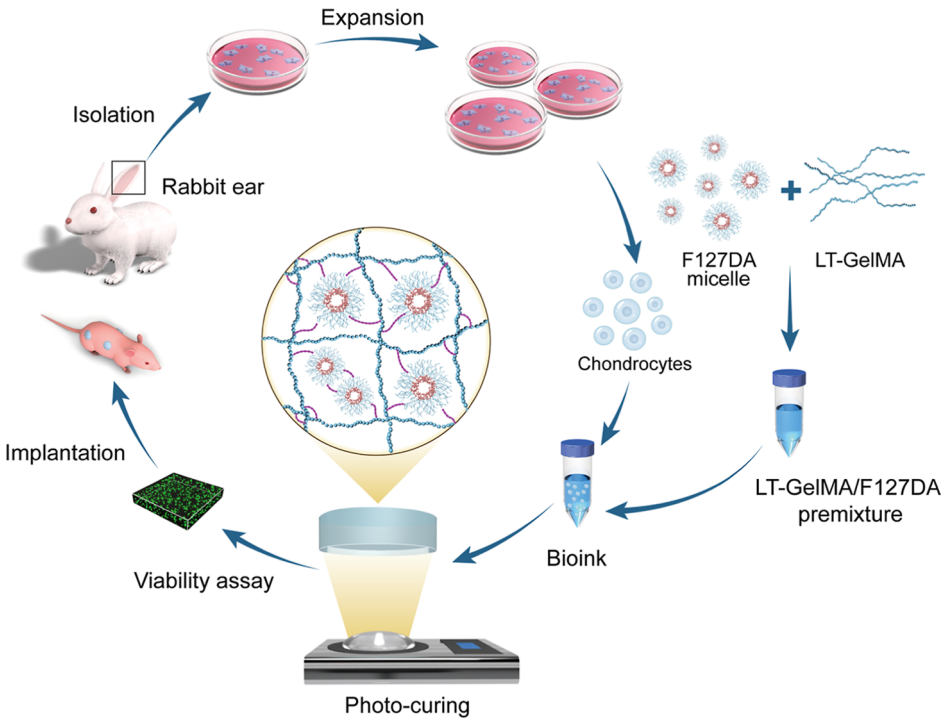

Figure 1. Schematic of LT-GelMA/F127DA bioink preparation and its application in cartilage regeneration. F127DA was incorporated into LT-GelMA to create a premixed solution. Chondrocytes were isolated and expanded from rabbit ears, then mixed with the LT-GelMA/F127DA premixture to prepare the bioink. The bioink was photo-cross-linked using a 405 nm curing light to form a dual-network structure in the shape of disk-like scaffolds. These scaffolds were subsequently cultured in vitro for cell viability assays and implanted subcutaneously into nude mice for in vivo experiments.

GelMA is distinguished by its unique nonthermosensitive property, which broadens its potential applications compared to thermosensitive GelMA. This innovative ichthyic-origin variant does not gel at room temperature (25 °C), even at concentrations ranging from 20% to 30% (w/v), thereby maintaining excellent fluidity.[24,25] LT-GelMA eliminates the need for high-temperature maintenance during use, offering distinct advantages in applications such as photocurable 3D printing, microneedle fabrication, and microfluidic microsphere production. Recent studies have demonstrated its utility in bioprinting, particularly for bone marrow mesenchymal stem cells and the creation of vascular-like networks, underscoring its versatility in advanced tissue engineering applications.[22] Despite these advantages, LT-GelMA faces a significant limitation in its mechanical strength, necessitating further optimization to expand its applicability in mechanically demanding contexts.

Pluronic F127-diacrylate (F127DA) is a modified triblock copolymer developed by introducing diacrylate groups at the terminal ends of Pluronic F127. This modification imparts photo-cross-linkable properties to the polymer, enhancing its utility in biomedical engineering applications.[26,27] F127DA's cross-linking capability significantly improves the structural stability and mechanical properties of hydrogels, making them well-suited for applications that demand mechanical resilience and structural fidelity over extended periods. Derived from Pluronic F127, a polymer recognized for its thermoreversible gelation and ability to form micellar structures, F127DA retains these unique features while broadening its applicability. These attributes make F127DA particularly valuable for creating robust and durable scaffolds that can withstand physiological stresses while maintaining an environment conducive to cellular activities and tissue regeneration. Additionally, its potential for controlled drug delivery and tissue engineering scaffold development further highlights its versatility in advanced biomedical applications.[28−30]

The primary objective of this study is to investigate the efficacy of a novel dual-network hydrogel system composed of LT-GelMA and F127DA in promoting the regeneration of ear cartilage (Figure 1). We hypothesize that the integration of LT-GelMA with F127DA in a dual-network hydrogel system synergizes their properties: LT-GelMA provides low-temperature solubility and enhanced biological functionality, while F127DA contributes robust mechanical properties and structural stability to the scaffold. We incorporated F127DA into LT-GelMA, systematically varying its concentration as the experimental variable. Through a photo-cross-linking reaction, carbon−carbon single bonds were formed, resulting in a dual-network structure. This configuration significantly enhances both the mechanical strength and structural stability of the hydrogel. By integrating these components, the system addresses the mechanical limitations of single-network LT-GelMA, offering a versatile platform for designing and optimizing scaffolds specifically tailored for cartilage reconstruction.[31,32]

2. RESULTS AND DISCUSSION

2.1. Preparation and Morphology. We developed a series of bioinks by blending different concentrations of F127DA with a constant concentration of LT-GelMA. During the preparation of LT-GelMA/F127DA hydrogels, we observed that the components remained fully soluble at low temperature (25 °C). In these hydrogel solutions, F127DA self-assembled into nanomicelles.[33] Upon addition of a

https://doi.org/10.1021/acsomega.5c00476
ACS Omega 2025, 10, 13570−13582

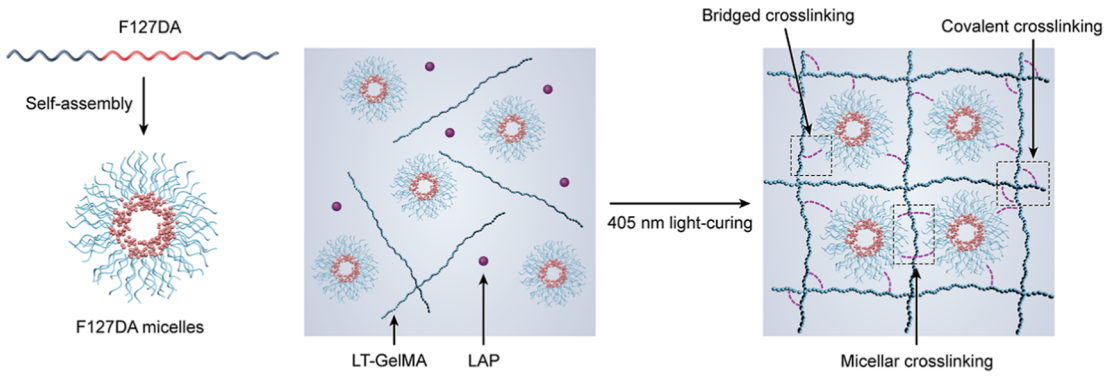

Figure 2. Schematic illustration of the preparation and cross-linking process of LT-GelMA/F127DA hydrogels. F127DA (represented by a two-color wavy line) self-assembles into nanomicelles (depicted as two-color sphere with red hydrophobic core and blue hydrophilic shell) in the hydrogel solution. Upon the addition of the photoinitiator LAP (shown as a purple ball) and exposure to 405 nm light, these micelles integrate with LT-GelMA (illustrated by a blue spiral) to form bonds (represented by purple dashed lines). The cross-linking process involves three critical interactions: micellar cross-linkings within F127DA nanomicelles, bridge linkages between F127DA nanomicelles and LT-GelMA, and direct covalent cross-linkings within LT-GelMA molecules. These interactions establish a robust dual-network structure.

photoinitiator and subsequent exposure to 405 nm light, these micelles integrated with LT-GelMA to form covalently cross-linked hydrogel networks.[31] This cross-linking process included micellar cross-linking within F127DA nanomicelles, bridging linkages between the F127DA nanomicelles and LT-GelMA, and the formation of direct covalent bonds within the LT-GelMA molecules (Figure 2). The Fourier transform infrared spectroscopy (FTIR) characterization results are presented in the Supporting Information (Figure S1).

Optical imaging of the bioinks before cross-linking revealed no significant change in color or transparency. The gross appearance after cross-linking showed that the transmittance decreased with higher concentration of F127DA (Figure 3A, up). SEM further elucidated the internal morphology and microporous structure of the hydrogels (Figure 3A, down). The hydrogels demonstrated a consistent and interconnected porous network, with no visible phase separation. Notably, hydrogels with F127DA exhibited more uniformly distributed pores. The average pore diameter ranged from 53.38 ± 14.17 to 100.32 ± 21.39 μm ($p < 0.001$), exhibiting an increasing trend with higher concentrations of F127DA (Figure 3B). In addition, Cryo-SEM images of the cross-linked LT-GelMA/F127DA hydrogels were available in the Supporting Information (Figure S2).

In summary, blending F127DA with LT-GelMA successfully formed covalently cross-linked hydrogels, and the transparency decreased with the increase of F127DA concentration. SEM analyses revealed a uniform, interconnected porous structure that became more defined as F127DA concentration increased, with larger pore diameters.

2.2. Characterization of LT-GelMA/F127DA Bioinks. We conducted compression tests to evaluate the compressive stiffness of our hydrogel scaffolds. The stress−strain curves for the four groups consistently showed that the compressive modulus increased with the concentration of F127DA (Figure 4A). Specifically, the modulus for the LG10 formulation was 21.41 ± 1.09 kPa, while it doubled to 43.89 ± 0.84 kPa ($p < 0.001$) for the LG10F2 formulation (Figure 4B). Our findings demonstrate that the incorporation of F127DA into the LT-GelMA hydrogel significantly enhances its compressive modulus.

Our rheological tests assessed the viscosity of bioinks with varying F127DA concentrations, all of which exhibited properties akin to Newtonian fluids. Specifically, bioinks with higher F127DA concentrations displayed increased viscosity. When subjected to a shear rate of 10 s^{-1} for 300 s, the viscosity remained stable, indicating no significant changes precuring (Figure 4C). Furthermore, the storage modulus (G') represents the elastic behavior, while the loss modulus (G'') reflects the viscous behavior of the material. Across the frequency range of 0.1 to 10 rad s^{-1}, G' of the bioinks consistently exceeded G'', and both moduli increased with higher F127DA concentrations, indicating that the material exhibits solid-like behavior with strong elastic characteristics under varying shear frequencies (Figure 4D, left). Time sweeps conducted at a constant strain and frequency (1% strain and 1 rad s^{-1}) for 300 s showed that G' remained higher than G'' for all bioinks, increasing with F127DA concentration. This result suggests the formation of a stable gel network dominated by elastic properties rather than viscous ones. The absence of significant fluctuations or crossover points between G' and G'' over time further supports the hydrogel's structural stability (Figure 4D, right). Rheological tests showed that bioinks with higher F127DA concentrations had increased viscosity and stable precuring properties.

We observed an inverse correlation between the swelling ratios of our cross-linked bioinks and the concentration of F127DA, which is essential for the long-term stability of hydrogel scaffolds. The base formulation, LG10, exhibited the highest swelling ratio at 4.15 ± 0.10. As the concentration of F127DA increased, the swelling ratio significantly decreased; for instance, LG10F2 demonstrated a reduced ratio of 3.40 ± 0.07, which was statistically significant ($p < 0.001$) (Figure 4E). These results indicate that higher concentrations of F127DA lead to a significant reduction in swelling ratio, suggesting enhanced structural integrity.

Our study examined the biodegradation of hydrogels in PBS solution, and found a notably slow degradation rate, which decreased further as the F127DA concentration increased from 0 to 2% w/v (Figure 4F). The LG10 formulation exhibited the most rapid degradation, losing nearly 20% of its mass within 7 days, while LG10F2 demonstrated remarkable stability, retaining over 75% of its mass after 28 days. The results indicated that the biodegradation of the hydrogels in PBS solution was slow and further diminished with increasing concentrations of F127DA.

https://doi.org/10.1021/acsomega.5c00476
ACS Omega 2025, 10, 13570−13582

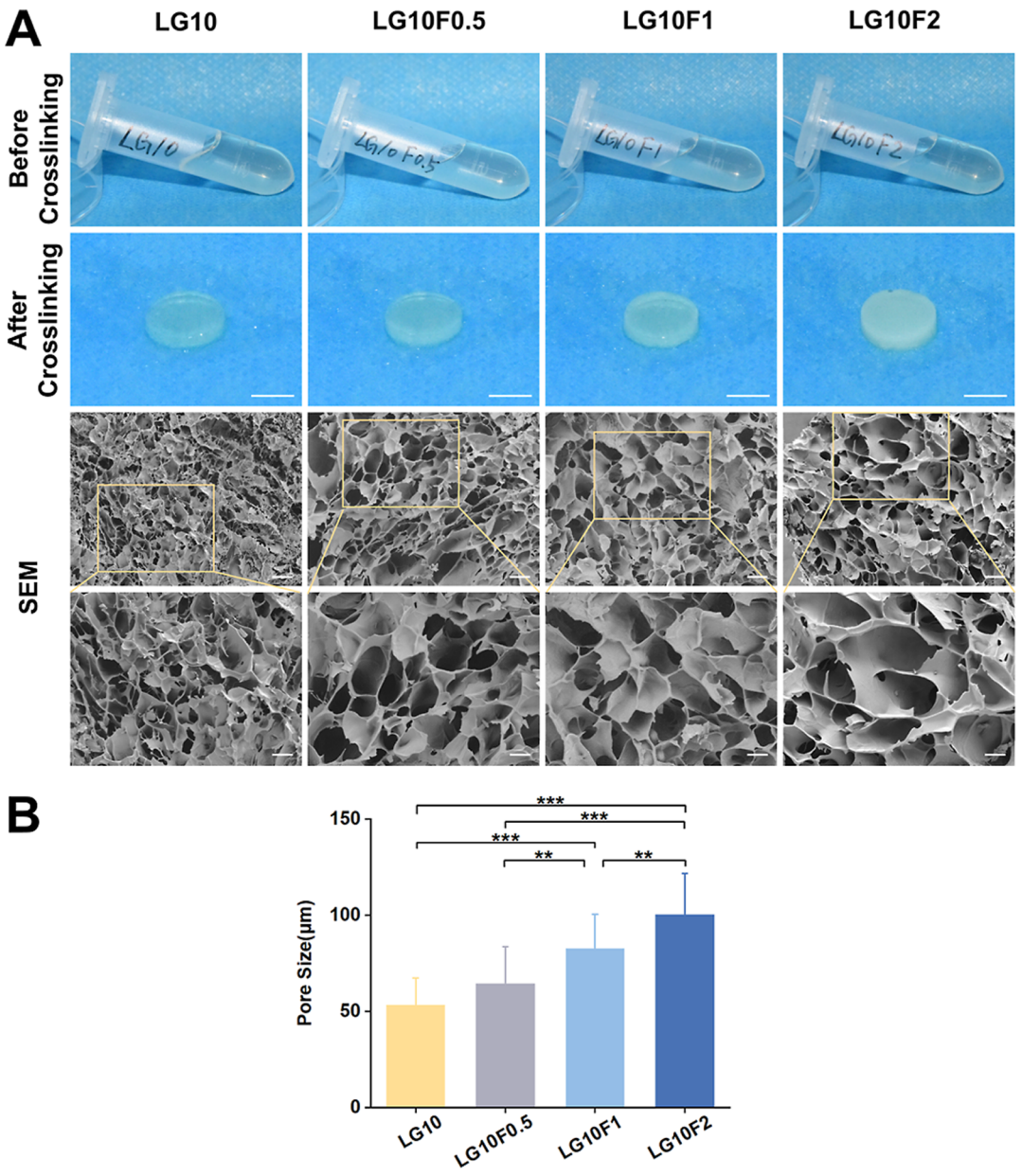

Figure 3. Morphology of the bioinks with different concentrations of F127DA. (A) The optical images of the bioinks before cross-linking show no significant differences in color or transparency. The gross appearance after cross-linking showed that the transmittance decreased with higher concentration of F127DA (scale bar: 5 mm). The SEM images provide a detailed view of the cross-linked LT-GelMA/F127DA hydrogels. At low magnification (scale bar: 100 μm), the overall porous structure is evident, with increased pore uniformity and size at higher F127DA concentrations. At high magnification (scale bar: 50 μm), the images reveal the enlargement of the pore size as F127DA concentration increases. (B) Quantitative analysis using ImageJ demonstrates a statistically significant increase in average pore size with rising F127DA concentrations (*p < 0.05, **p < 0.01, ***p < 0.001).

2.3. Cell Culture In Vitro. We assessed the viability of chondrocytes cultured within disk-like scaffolds using live/dead staining at days 1 and 7 (Figure 5A). Initially, cell viability exceeded 95% after 1 day of culture across all samples, as analyzed by NIS-Elements AR software. This high viability rate indicates minimal impact from the photo-cross-linking treatment on cell survival (Figure 5B, day 1). By day 7, groups containing F127DA displayed enhanced cell viability compared to those with solely LT-GelMA, and viability improved further with increasing concentrations of F127DA (p < 0.001) (Figure 5B, day 7). These results suggest that F127DA positively influences cell viability. Overall, the LT-GelMA/F127DA hydrogel demonstrated excellent biocompatibility, making it suitable for cell encapsulation applications.

2.4. Neocartilage Formation In Vivo. To ensure the practical applicability of our cell-laden scaffolds, it is crucial that they remain stable not only during in vitro culture but also continue to mature when implanted in vivo.[34] We investigated this by implanting chondrocyte-laden scaffolds into a subcutaneous nude mice model, monitoring the tissue's stability and maturation over 4 and 8 weeks (Figure 6A). The results of representative animals from the in vivo experiments are presented in the Supporting Information (Figure S3). It was found that all scaffold groups maintained structural integrity with a tough and elastic texture at 4 weeks

https://doi.org/10.1021/acsomega.5c00476
ACS Omega 2025, 10, 13570−13582

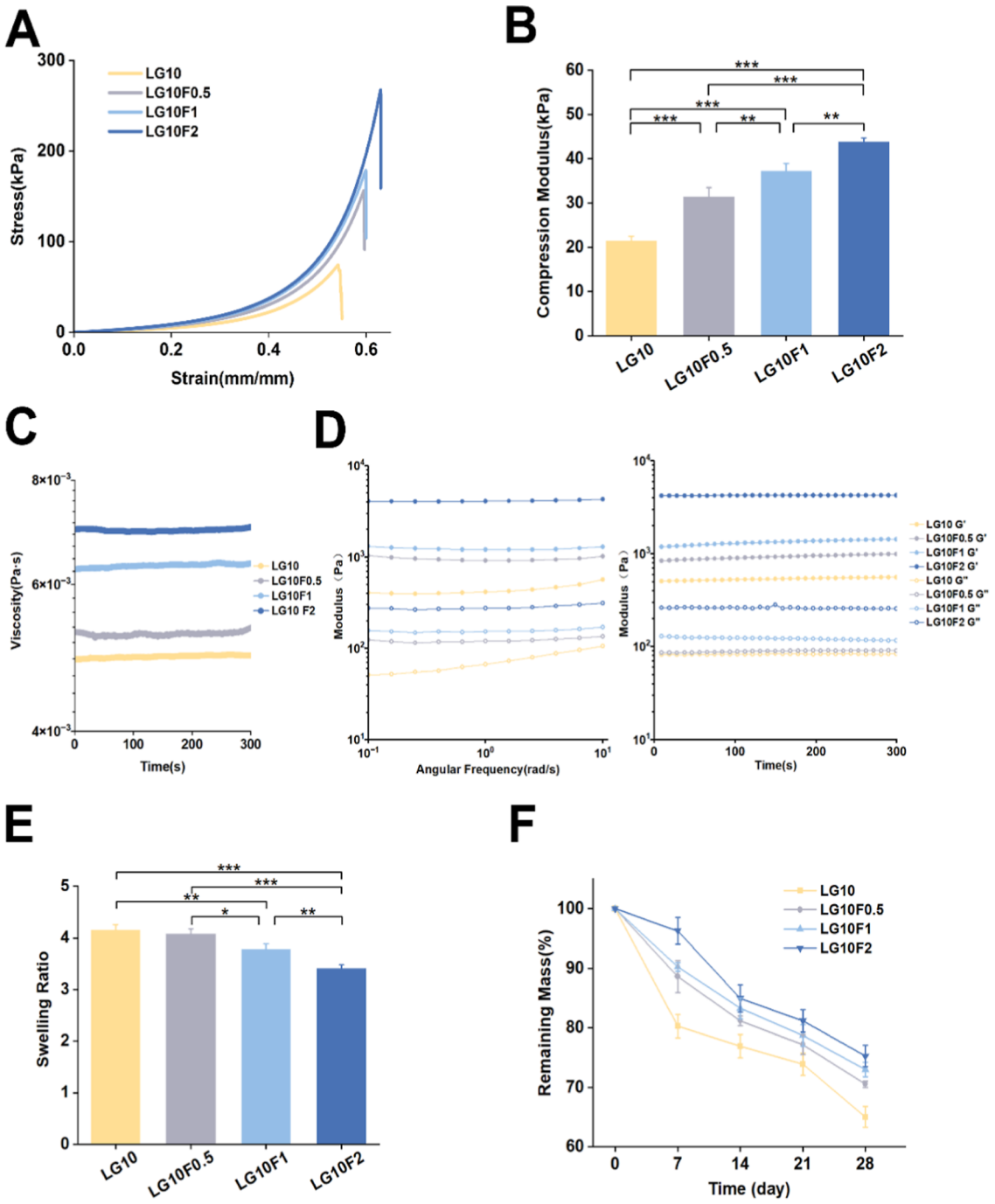

Figure 4. Characterization of LT-GelMA/F127DA bioinks with varying F127DA concentrations. Different colors or lines correspond to bioinks with varying F127A concentrations. (A) Stress−strain curves: This panel illustrates the stress−strain behavior of the bioinks under compressive loading, revealing that the compressive modulus increases with higher F127DA concentrations. The curve's shape provides insight into the material's mechanical strength and elasticity, where steeper slopes indicate higher stiffness. (B) Compressive modulus: The compressive modulus, calculated from the linear region of the stress−strain curves, is plotted here as a bar graph. The compressive modulus increases significantly as the concentration of F127DA increases, demonstrating the enhancement of mechanical stiffness due to F127DA incorporation. (C) Viscosities of precuring bioinks: This subplot presents the viscosity of the bioinks before curing, measured as a function of shear rate. The curves show that bioinks with higher F127DA concentrations exhibit increased viscosity, maintaining stability over time. A lower viscosity indicates a thinner, less resistant bioink to flow. (D) Storage (G') and loss (G'') modulus: the storage modulus (G') and loss modulus (G'') of the bioinks are plotted as a function of angular frequency. G' represents the elastic behavior and G'' indicates the viscous behavior. Both moduli increase as the F127DA concentration rises. A higher G' compared to G'' suggests a more solid-like material, which is beneficial for structural stability postcuring. (E) Swelling ratio: This bar graph illustrates the swelling ratio of the hydrogels after immersion in PBS for a specified time. The swelling ratios of the cross-linked bioinks decrease inversely with increasing F127DA concentrations, highlighting improved structural integrity. (F) In vitro degradation: The remaining mass of the hydrogels is depicted as a function of time. The biodegradation profile in PBS solution reveals a slower degradation rate with higher F127DA concentrations, demonstrating enhanced longevity and stability (*$p < 0.05$, **$p < 0.01$, ***$p < 0.001$).

https://doi.org/10.1021/acsomega.5c00476
ACS Omega 2025, 10, 13570−13582

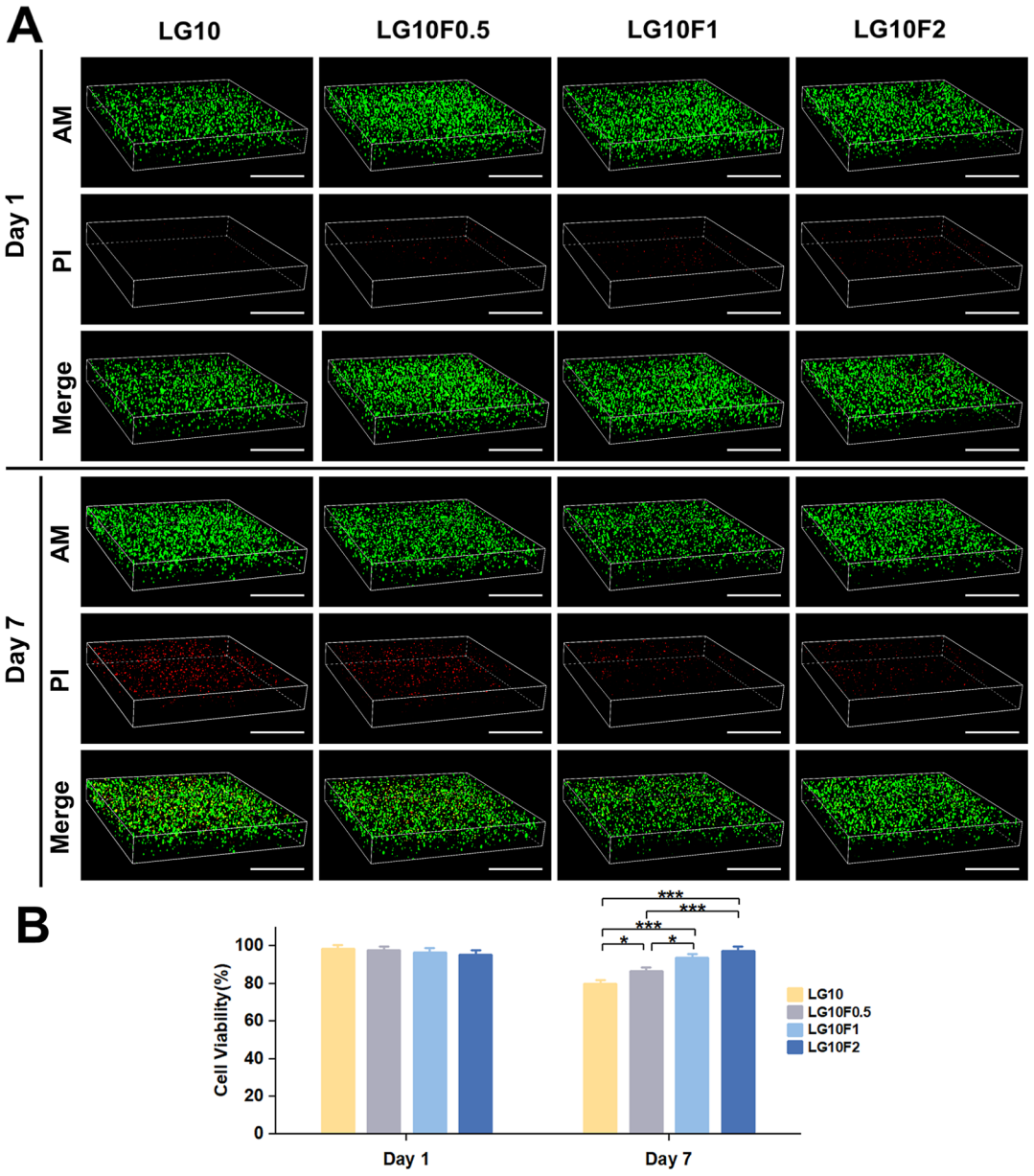

Figure 5. Results of in vitro culture of chondrocytes within LT-GelMA/F127DA bioink-based photo-cross-linked constructs. (A) 3D reconstructed confocal fluorescence images show the constructs at days 1 and 7. Live/Dead staining was performed to assess cell viability (scale bar: 500 μm). Green fluorescence indicates live cells, while red fluorescence marks dead cells. The images reveal high cell viability at day 1, with minimal red staining, and a significant increase in viability with increasing concentrations of F127DA at day 7. (B) Quantitative analysis of chondrocyte viability confirms the observations, showing high rates (>95%) at day 1 for all samples and a statistically significant increase at day 7, with constructs containing F127DA outperforming those with only LT-GelMA (*$p < 0.05$, **$p < 0.01$, ***$p < 0.001$).

(Figure 6B, week 4). By 8 weeks, however, the grafts became denser and their texture less smooth (Figure 6B, week 8).

Histological evaluations were performed at both 4 and 8 weeks post-transplantation using H&E, Safranin O, Toluidine Blue, and Collagen II staining techniques (Figure 6C). These analyses showed that chondrocytes within the scaffolds formed lacuna-like structures, indicative of early cartilage formation. Notably, the hydrogels facilitated the secretion of glycosaminoglycan (GAG) and type II collagen, both essential for cartilage regeneration.[35] At week 4, chondrocytes were organized in clusters within lacunae, surrounded by the extracellular matrix they secreted. At week 8, an increase in cell density and the visibility of cartilage lacunae were observed, along with the presence of brown-stained type II collagen fibers, indicating the formation of new cartilage tissue. Furthermore, the area positive for type II collagen staining increased progressively with higher concentrations of F127DA at both 4 and 8 weeks ($p < 0.05$) (Figure 6D). These findings suggest that the LT-GelMA/F127DA hydrogel effectively supports chondrocyte survival and chondrogenesis in vivo. Overall, our results indicate superior cartilage regeneration capabilities, particularly in the LG10F2 group, highlighting the potential of this hydrogel system for clinical applications in cartilage tissue engineering.

This study investigates the potential of LT-GelMA and F127DA composite hydrogels for cartilage regeneration, both in vitro and in vivo. Our findings demonstrate a significant improvement in cartilage tissue formation, supporting our

https://doi.org/10.1021/acsomega.5c00476
ACS Omega 2025, 10, 13570−13582

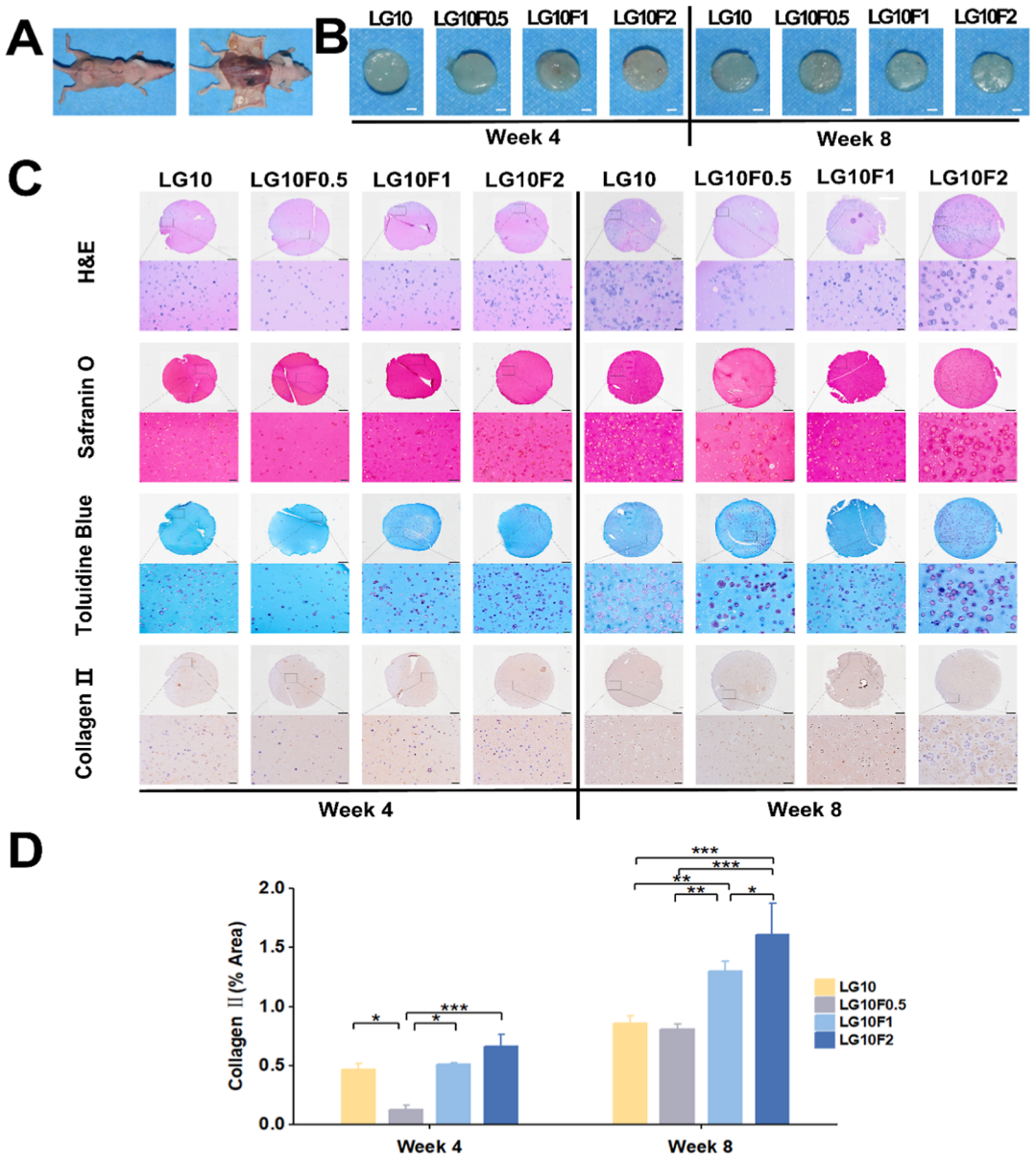

Figure 6. In vivo neocartilage formation. (A) Top: picture taken right after the subcutaneous implantation of auricular. Bottom: picture taken during explantation of constructs after 8 weeks in vivo. (B) Images of in vivo constructs at weeks 4 and 8 (scale bar: 2 mm). (C) In vivo histological analysis for the development of cartilage tissue formation at 4 and 8 weeks after transplantation. Histological and immunohistological analyses for H&E, Safranin O, Toluidine Blue and Collagen II at low magnification (scale bar: 1 mm) and at high magnification (scale bar: 100 μm). (D) Collagen II positive staining area analysis of chondrocytes in constructs at weeks 4 and 8 (*$p < 0.05$, **$p < 0.01$, ***$p < 0.001$).

initial hypothesis that the biochemical properties of LT-GelMA, combined with the physical stability of F127DA, promote chondrogenesis.

The increase in pore size with higher F127DA concentrations can be attributed to alterations in the hydrogel's properties during freeze-drying. We speculate that the incorporation of F127DA modifies the overall hydrogel properties, potentially by influencing the physical interactions between polymer chains and the freezing process. A recent study demonstrated that the formation of an internal porous structure during hydrogel freeze-drying is highly dependent on ice nucleation, where the size of ice crystals plays a critical role.[36] As the F127DA concentration increases, it likely alters the nucleation behavior during freezing by introducing additional interfacial interactions between polymer chains. As a block copolymer, F127DA may disrupt the uniformity of ice crystal formation, leading to the development of larger ice crystals and, consequently, larger pores in the freeze-dried hydrogel. However, the precise mechanism linking F127DA concentration to pore size variation requires further investigation. The incorporation of F127DA significantly increased the average pore diameter, thereby enhancing the biocompatible properties of the hydrogels.[37] Structural modifications, such as changes in pore size within tissue engineering scaffolds, play a crucial role in supporting cell viability.[38,39] These enhancements improve cell viability by providing larger spaces for cell-to-cell interactions and nutrient exchange, facilitating improved cell adhesion, proliferation, and migration.[40,41] Furthermore, the low-temperature solubility of these hydrogels offers practical advantages for clinical applications, allowing for preparation at lower temperatures and eliminating the need for continuous heating during use. This property is particularly

https://doi.org/10.1021/acsomega.5c00476
ACS Omega 2025, 10, 13570−13582

important for applications requiring high fluidity and high-concentration tissue engineering scenarios.

The observed increase in stiffness is directly linked to the enhanced cross-linking within the hydrogel network between GelMA and F127DA. As the concentration of F127DA increased, the cross-linking density also increased, which elevated the elastic modulus of the hydrogel, thereby improving its mechanical properties.[31,42] F127DA not only increased the loss modulus before cross-linking but also enhanced the storage modulus after cross-linking. The dominance of G' over G'' confirms that the hydrogel possesses a stable and resilient network structure under the tested frequency conditions. The stability of G' across frequencies indicates that the hydrogel can withstand varying shear stresses without significant structural compromise. This behavior is particularly advantageous for applications requiring structural stability, such as 3D printing or load-bearing tissue scaffolds. Furthermore, the consistent dominance of G' over G'' across the observed time frame highlights the hydrogel's ability to maintain structural integrity, a critical feature for applications demanding sustained mechanical performance. The demonstrated rheological stability suggests the hydrogel's suitability for applications where consistent mechanical properties are essential, such as in tissue engineering or drug delivery systems. The low viscosity of the bioinks is advantageous for easy mixing of cells into the hydrogel prior to gelation, ensuring uniform cell distribution within the matrix, which is essential for consistent cell function and effective tissue regeneration.[43] Additionally, the low viscosity supports minimally invasive applications, enabling precise injection without the need for open surgery. This approach significantly reduces recovery times, healthcare costs, and the risks of patient discomfort and infection.[44] The hydrogel's stable rheological behavior, akin to a near-Newtonian fluid, further enhances its biocompatibility and minimizes the risk of mechanical irritation to adjacent tissues.[45]

Lower swelling rates are crucial for maintaining the structural integrity of hydrogel scaffolds. By limiting excessive expansion after implantation, these rates help prevent mechanical mismatches with surrounding tissues, which could otherwise lead to the delamination or failure of the implanted material.[46] Controlled swelling behavior not only ensures better compatibility with native cartilage but also reduces the risk of inflammatory responses, thereby improving the integration of the engineered tissue with host cartilage. The incorporation of F127DA into the scaffolds not only reduced the degradation rate compared to scaffolds composed solely of LT-GelMA but also enhanced the complexity of the hydrogel's 3D structure through increased cross-linking. This structural stability is advantageous for cell proliferation, adhesion, and extracellular matrix (ECM) production.[47] The robust network formed by F127DA photo-cross-linking was particularly resistant to degradation in PBS, highlighting the hydrogel's excellent biocompatibility and its potential for maintaining structural integrity during short-term implantation in clinical settings.

The LT-GelMA/F127DA hydrogel exhibited strong potential for cartilage tissue engineering, as evidenced by high initial chondrocyte viability and improved cell survival over time, particularly at higher F127DA concentrations. This suggests that F127DA positively influences cell health, likely by enhancing the scaffold's mechanical properties and constructing a more favorable microenvironment for cell proliferation. In vivo studies further confirmed these findings, demonstrating that the hydrogel maintained structural integrity and promoted neocartilage formation, with significant increases in glycosaminoglycan and type II collagen production, especially in the LG10F2 formulation. Although LG10F1 exhibits more intense chondrogenic staining (Safranin O, Toluidine Blue), LG10F2 demonstrates superior performance in terms of cartilage cell quantity and maturity. Additionally, LG10F2 possesses enhanced mechanical properties and a more controlled biodegradation rate, both of which are critical for long-term cartilage regeneration and functional applications. Therefore, while LG10F1 shows promising chondrogenic potential, LG10F2 provides a more balanced and favorable profile when considering all aspects of cartilage tissue engineering. These results indicate that the LT-GelMA/F127DA hydrogel is a promising candidate for clinical applications in cartilage regeneration.

When comparing LT-GelMA/F127DA hydrogels with similar systems reported in the literature, several key aspects should be considered. This study focuses on the novel material LT-GelMA and strategies to improve its mechanical strength. By combining LT-GelMA with F127DA, we developed a dual-network hydrogel that enhances mechanical strength while preserving the unique nonthermosensitive property of LT-GelMA. The primary advantage of the LT-GelMA/F127DA system is its low-temperature solubility, with the addition of F127DA significantly improving mechanical strength, degradation time, and other properties compared to LT-GelMA alone. Unlike the GelMA/PEGDA/F127DA system, the LT-GelMA/F127DA hydrogel in our study maintains excellent fluidity at room temperature, enabling convenient usage without the need for heating. Furthermore, in contrast to studies that seeded cells onto scaffold surfaces, our in vitro and in vivo experiments employed a 3D culture approach by encapsulating cells within the hydrogel.[48] This method more closely simulates the cellular growth environment within tissues, enhancing the reliability and relevance of our findings. The preparation and cross-linking methods of LT-GelMA/F127DA hydrogels are unique due to the dual-network approach that integrates micellar cross-linking with covalent bonds, providing a structural advantage over conventional single-network hydrogels.[31] Studies on comparable systems have shown that such dual-network hydrogels typically exhibit enhanced mechanical properties, which is consistent with the increased compressive and storage moduli observed in our study.[49,50] The LT-GelMA/F127DA hydrogels exhibit controlled swelling behavior and slower degradation, which can be advantageous for providing sustained structural support in tissue engineering. This contrasts with some previous studies where faster degradation rates have been reported, potentially compromising scaffold integrity.[33] Regarding biocompatibility, our hydrogels show high cell viability, consistent with outcomes reported for other hydrogels in cartilage tissue engineering.[51] In vivo, the neocartilage formation and integration achieved with our hydrogels are comparable to, or even better than, those of other systems, likely due to the optimized mechanical and rheological properties that more closely mimic native cartilage.[31,49]

Despite these promising findings, there are limitations to this study that should be addressed in future research. The short duration of the in vivo experiments and the use of nude mice may limit the generalizability of the results. Future studies should investigate the long-term effects and validate these

https://doi.org/10.1021/acsomega.5c00476
ACS Omega 2025, 10, 13570−13582

findings in larger animal models or clinical trials. Moreover, expanding the range of F127DA concentrations tested could offer additional insights into optimizing the hydrogel's properties. Addressing these limitations will be crucial for advancing the clinical application of this hydrogel in cartilage repair and other regenerative therapies.

Recent advancements in tissue engineering have highlighted the potential of cartilage organoids, which offer a more sophisticated approach to replicating the complex structure and function of native cartilage tissue. Cartilage organoids are 3D constructs that more accurately mimic the cellular environment, ECM interactions, and mechanical properties of cartilage, which are often challenging to reproduce in traditional 2D cell culture systems. The use of cartilage organoids enables more precise modeling of cartilage growth, differentiation, and tissue repair processes, providing a promising avenue for enhancing cartilage regeneration strategies. Their development relies heavily on biomimetic scaffolds, particularly hydrogels such as alginate, peptides, and silk fibroin, which provide an ECM-like environment conducive to chondrogenesis.[52,53] Moreover, advanced bioengineering approaches, including studies on endogenous stem cell-driven cartilage regeneration and the exploration of decellularized ECM-based bioinks for 3D bioprinting, further demonstrate the potential for improved cartilage repair strategies.[54,55] Cartilage organoids hold tremendous promise in advancing cartilage tissue engineering and regenerative medicine. The integration of hydrogels, advanced bioengineering techniques, and biomimetic scaffolds presents exciting opportunities for improving cartilage repair. Continued research into optimizing hydrogel formulations and expanding the application of organoids will significantly contribute to the development of more effective and sustainable treatments for cartilage defects and degenerative diseases.

Overall, the LT-GelMA/F127DA dual-network hydrogels developed in this study exhibit improved mechanical properties, controlled degradation rates, and excellent biocompatibility. These advantages make them highly promising candidates for translation into clinical applications. The enhanced structural stability and tunable properties of these hydrogels address key challenges associated with cartilage tissue engineering, providing a robust platform for scaffold design. The results of this study underscore the strong potential of LT-GelMA/F127DA hydrogels for advancing cartilage repair and regeneration, paving the way for their application in clinical settings.

3. CONCLUSIONS

This study presents the development of a novel dual-network hydrogel composed of LT-GelMA and F127DA. This innovative hydrogel combines low-temperature solubility with optimized mechanical properties and degradation rates through the incorporation of photo-cross-linkable nanomicelles. In vitro and in vivo experiments confirm its excellent performance in tissue-engineered cartilage construction. This dual-network hydrogel emerges as a promising candidate for cartilage tissue engineering scaffolds, offering an effective solution for cartilage regeneration.

4. MATERIALS AND METHODS

4.1. Materials. LT-GelMA (EFL-LG-101) and F127DA (EFL-F127DA-001), along with the photoinitiator lithium phenyl-2,4,6-trimethylbenzoylphosphinate (LAP) (EFL-LAP), and the Live & Dead Viability Assay Kit (EFL-CLD-001), were obtained from Engineering For Life (EFL, China). Trypsin-EDTA Solution (C0201) was sourced from Beyotime (China). Collagenase NB 4 standard grade (S1745401) was purchased from Nordmark (Germany). High glucose Dulbecco's Modified Eagle Medium (H-DMEM) (SH30243.01) and fetal bovine serum (FBS) (SV30208.02) were acquired from Hyclone (USA). Gentamicin sulfate solution (MA0322) and amphotericin B (A1264) were procured from MeilunBio and Gentihold (China), respectively. Staining kits for Hematoxylin−Eosin (HE) (G1120), safranin O (G2540), and toluidine blue (G2543) used for cartilage staining were supplied by Solarbio (China). Collagen type II polyclonal antibody (28459−1-AP) and IHC Prep & Detect Kit for Rabbit/Mouse Primary Antibody (PK10019) were purchased from Proteintech (USA).

4.2. Cell Isolation and Expansion. Auricular cartilage tissues were obtained from Japanese white rabbits under sterile conditions, with all procedures approved by the Institutional Animal Care and Use Committee (IACUC) of Jilin University (approval number: SY202405008). The tissues were meticulously cleaned and disinfected, immersed in sterile saline containing 2 mg mL^{-1} gentamycin and 0.025 mg mL^{-1} amphotericin B, and then dissected to remove the skin, subcutaneous tissue, and perichondrium. The cleaned tissues were then segmented into 1 mm^3 pieces.

Chondrocytes were isolated using 0.25% trypsin including 0.02% ethylene diamine tetraacetic acid (EDTA) for 0.5 h and 0.2% collagenase NB 4 standard grade for 20 h, both processes taking place at 37 °C. The resulting solution was filtered through a 70 μm cell strainer and the filtrate collected in a 50 mL centrifuge tube. This was followed by centrifugation at 1500 rpm for 10 min, repeated three times, to remove the supernatant.

The cell pellet was resuspended in H-DMEM (4500 mg L^{-1} glucose, 4.00 mM L-glutamine, 110 mg L^{-1} sodium pyruvate) supplemented with 10% FBS and 0.2 mg mL^{-1} gentamycin. The primary chondrocytes were then seeded in 10 cm cell culture dishes (Biofil, China) and cultured at 37 °C in a 5% CO_2 environment. Cells were subcultured upon reaching confluence, with the medium refreshed every 3 days, to support continued growth and expansion.

4.3. Preparation of Hydrogel Scaffolds. All procedures were performed at room temperature. LT-GelMA was dissolved in phosphate buffer solution (PBS) at 20% w/v by gentle stirring until fully dissolved. F127DA was dissolved separately in PBS at 2%, 4%, 8% w/v by stirring until a clear solution was obtained. LAP was dissolved in PBS at 1% w/v with stirring until a clear solution was achieved. Then, 20% LT-GelMA, 1% LAP and various concentrations F127DA solution were mixed evenly at the volume ratio of 2:1:1, respectively. The F127DA solution was slowly added to the 20% LT-GelMA solution under continuous stirring. The mixture was stirred for 10 min to ensure homogeneity. Then, 1% LAP was added to the LT-GelMA/F127DA mixture to achieve a final concentration of 0.25% w/v. The solution was stirred again for 5 min to ensure uniform distribution of the photoinitiator. In the control group, F127DA was replaced by an equal volume of PBS. After completing the above steps, four formulations of uniform and transparent hybrid solution were obtained: 10% LT-GelMA (LG10, the control group), 10% LT-GelMA with 0.5% F127DA (LG10F0.5), 10% LT-GelMA

https://doi.org/10.1021/acsomega.5c00476
ACS Omega 2025, 10, 13570−13582

with 1% F127DA (LG10F1), and 10% LT-GelMA with 2% F127DA (LG10F2). Care should be taken to avoid exposure to light after the addition of a photoinitiator. Results of preliminary experiments and the rationale for selecting the optimal F127DA concentration are clarified in the Supporting Information (Figure S4).

After thoroughly mixing and dissolving the solutions, they were filtered through a 0.22 μm filter to eliminate bacterial contamination. 150 μL of each of the above hydrogel solutions were then loaded into sterile cylindrical molds fashioned from syringes and cured under 405 nm light (EFL-LS-1601, EFL, China) for 2 s, forming disk-like scaffolds with an 10 mm diameter and 2 mm thickness.

4.4. Scanning Electron Microscopy. To analyze the microstructure of the LT-GelMA/F127DA hydrogel scaffolds from the four experimental groups, samples were lyophilized using a lyophilizer (LyoQuest, Telstar, Spain). Initially, all samples were frozen at −80 °C for 2 h to ensure complete solidification. The frozen samples then underwent a primary drying phase at −80 °C and 0.2 mbar for 18 h, during which the majority of the water content was sublimated. This was followed by a secondary drying phase at 25 °C under the same pressure for 2 h to remove residual moisture. The dried samples were sputter-coated with a current of 20 mA for 150 s and subsequently transferred to the SEM stage for observation. The surface morphology of each scaffold type was examined using a scanning electron microscope (Sigma 300, Zeiss, Germany). For quantitative analysis, the average pore size of the hydrogels was measured using ImageJ software.

4.5. Compression Testing. The mechanical properties of the hydrogel scaffolds from four different groups were evaluated using an electrical universal material testing machine (5944 MicroTester, Instron, USA). Prior to testing, the samples were equilibrated in PBS at 37 °C for 24 h to ensure uniformity. The cylindrical scaffolds, each measuring 10 mm in diameter and 4 mm in height, were aligned vertically between two parallel plates. During testing, the samples were compressed to 60% of their original height at a consistent rate of 1 mm/min. This procedure was replicated three times independently for each group to ensure consistency and reliability of the results. A power analysis based on preliminary studies was typically performed to estimate the minimum sample size for compression test. The compressive modulus for each scaffold was determined by analyzing the slope of the linear region of the stress−strain curves, specifically between 5% and 15% strain.

4.6. Rheological Examination. Rheological testing was carried out using a hybrid rheometer (Discovery HR-2, TA Instruments, USA) at 25 °C. First, the viscosity of the hydrogel solution was assessed by placing it between parallel plates and applying a shear rate of 10 s^{-1} for 300 s. Subsequently, the solution was formed into a gel sheet (10 mm in diameter and 1 mm in height). The storage and loss moduli of the gel were then determined through time sweep experiments, which were conducted at consistent strain (1%) and frequency (1 rad s^{-1}) for 300 s. Additionally, frequency sweep tests were performed within the range of 0.1−10 mL $^{-1}$, maintaining a shear strain of 1% to further characterize the rheological properties of the hydrogel.

4.7. Swelling Ratio. To measure the swelling ratios of the hydrogel scaffolds, the following procedures were implemented. Disc-shaped specimens, each 10 mm in diameter and 2 mm in height, were prepared using the hydrogels with varying F127DA concentrations. The specific procedure of lyophilization was the same as described in SEM part. After lyophilization, each sample was weighed (denoted as M1). The samples were then immersed in PBS at 37 °C for 24 h and subsequently reweighed (denoted as M2). The swelling ratio (SR) for each sample was calculated using the formula SR = (M2−M1)/M1. This process was replicated three times. The sample size was determined statistically using power analysis based on preliminary data.

4.8. In Vitro Degradation. The in vitro degradation of LT-GelMA/F127DA hydrogels was assessed through weight loss measurements in a pH 7.4 phosphate buffer solution (PBS) at 37 °C. Initially, the hydrogels from each of the four groups were freeze-dried, weighed, and denoted as W1. Samples from each group were then placed in a 24-well cell culture plate, each well containing 1 mL of PBS. This plate was kept on a shaking table at 37 °C, with the PBS refreshed every 3 days.

Following incubation periods of 7, 14, 21, and 28 days, the scaffolds were again lyophilized and reweighed, recorded as W2. The percentage of mass remaining after each period was calculated using the formula: remaining mass (%) = (W2/W1) × 100. This procedure was performed in triplicate. Replicates for each test were calculated using power analysis based on preliminary data.

4.9. In Vitro Culture. For the in vitro culture experiments, chondrocytes at passage two were utilized. The cells were detached with a trypsin/EDTA solution, collected by centrifugation, counted with a hemocytometer. The cells were subsequently resuspended in each of the four different hydrogel solutions to achieve a cell density of 1×10^7 cells/ml.

This cell suspension was used to prepare cell-laden hydrogel scaffolds following the previously described methods. The resulting scaffolds were cultured in H-DMEM supplemented with 10% FBS and 0.2 mg mL^{-1} gentamycin at 37 °C in a humidified atmosphere containing 5% CO_2. The hydrogels were maintained in this medium, with medium being refreshed every 3 days to maintain optimal growth conditions.

4.10. Cell Viability Assay. To assess the viability of chondrocytes embedded within the hydrogels, live/dead staining was performed using the live & dead viability assay kit. Initially, calcein-AM and propidium iodide (PI) were diluted with PBS to prepare the working solutions. The cell-laden hydrogel discs were cultured in the same medium and conditions for one and 7 days, after which they were rinsed three times with PBS.

Subsequently, the discs were incubated with the PI working solution (10 μM) for 10 min, followed by a PBS rinse to remove excess PI. Next, calcein-AM working solution (2 μM) was added, and the samples were incubated for an additional 45 min at room temperature in the dark. After incubation, the hydrogel discs were again rinsed with PBS to remove excess dye and immediately imaged using a laser confocal microscope (AXR, Nikon, Japan) to assess cell viability. Live cells were stained green (calcein-AM), while dead cells were stained red (PI). The z-axis scan length was set at 250 μm. This assay was conducted in triplicate, with the cell viability quantified by averaging results from three randomly selected images per sample.

4.11. Subcutaneous Nude Mice Implantation. Experiments involving nude mice were conducted in compliance with the ethical guidelines approved by the IACUC of Changchun Weishi Testing Technology Service Co., Ltd. (approval

https://doi.org/10.1021/acsomega.5c00476
ACS Omega 2025, 10, 13570−13582

number: 20240425-01). Female BALB/c-nu nude mice, aged 6−8 weeks and weighing 18 to 20 g, were sourced from Beijing Vital River Laboratory Animal Technology Co., Ltd., China. Twenty mice were randomly divided into two groups (n = 10 mice per group). Hydrogel scaffolds laden with chondrocytes, namely, LG10, LG10F0.5, LG10F1, and LG10F2, were prepared under sterile conditions and presoaked in complete medium.

For implantation, the mice were anesthetized using isoflurane at 1% in oxygen. The surgical area was marked and sterilized with 0.5% povidone-iodine and 75% ethanol. Two 15 mm incisions were made along the dorsal midline, creating four subcutaneous pockets through blunt dissection. The chondrocyte-laden scaffolds were gently implanted into these pockets. The incisions were then closed with intermittent 5−0 cosmetic sutures to secure the scaffolds in place and prevent structural damage.

Mice were monitored in a temperature-controlled environment until they fully recovered from anesthesia. Postoperative care included administering buprenorphine at 0.05 mg/kg every 12 h for 48 h to alleviate pain. The animals were housed individually and observed daily for signs of distress, infection, or abnormal behavior. The surgical site was regularly inspected, and wound healing was closely monitored.

From days 1−3 postimplantation, the mice were monitored daily for incision healing and overall health. During the first week, visual inspections and palpation of the implantation site were performed to detect any signs of swelling, redness, or abnormal tissue growth. In weeks 2 through 4, the focus shifted to evaluating implant integration and potential immune responses. At 4 and 8 weeks postimplantation, five mice from each group were randomly euthanized, and the implanted scaffolds were harvested for histological analysis.

4.12. Histological Evaluation. Immediately after harvesting, the specimens were fixed in a paraformaldehyde solution, subsequently dehydrated, and embedded in paraffin. For staining, the samples underwent hematoxylin and eosin (H&E), safranin O, and toluidine blue staining. Immunohistochemical analyses were performed using Collagen type II polyclonal antibody (1:800), followed by polymer HRP-goat antirabbit/mouse secondary antibody to detect Collagen II. The area showing positive Collagen II staining in the constructs at weeks 4 and 8 was quantified using ImageJ software.

4.13. Statistical Analysis. All data are presented as mean ± standard deviation. Prior to conducting analysis of variance (ANOVA), the normality of the data was assessed using Shapiro−Wilk test. To evaluate the homogeneity of variances across groups, Levene's test was applied. For posthoc pairwise comparisons, Tukey's test was used if the assumptions of normality and equal variances were satisfied. In cases where these assumptions were not met, alternative methods such as Bonferroni correction were employed to account for multiple comparisons and control for Type I error. All statistical analyses were performed using Origin 2024 software. Statistical significance was determined by a p-value of less than 0.05.

■ ASSOCIATED CONTENT

Data Availability Statement

The authors declare that all data supporting the results of this study are available in the article and its Supporting Information files or can be obtained from the corresponding author upon reasonable request.

Supporting Information

The Supporting Information is available free of charge at https://pubs.acs.org/doi/10.1021/acsomega.5c00476.

FTIR characterization results; effect of freezing temperature on hydrogel pore size; in vivo animal experiments; preliminary in vitro experiments (PDF)

■ AUTHOR INFORMATION

Corresponding Authors

Tian Li − *Department of Plastic and Reconstructive Surgery, The First Hospital of Jilin University, Changchun 130021, China;* orcid.org/0000-0003-3578-6464; Email: litian@jlu.edu.cn

Duo Zhang − *Department of Plastic and Reconstructive Surgery, The First Hospital of Jilin University, Changchun 130021, China;* orcid.org/0000-0002-7372-6799; Email: zhangduo@jlu.edu.cn

Authors

Bingzhang Liu − *Department of Plastic and Reconstructive Surgery, The First Hospital of Jilin University, Changchun 130021, China*

Yuhan Jiang − *Department of Plastic and Reconstructive Surgery, The First Hospital of Jilin University, Changchun 130021, China*

Yufeng Tian − *Department of Plastic and Reconstructive Surgery, The First Hospital of Jilin University, Changchun 130021, China*

Complete contact information is available at: https://pubs.acs.org/10.1021/acsomega.5c00476

Author Contributions

D.Z. and T.L. contributed equally to this work and should be considered co- corresponding authors. D.Z. and T.L. conceived and designed the experiments. B.L. was responsible for experiments, data analysis and manuscript preparation. Y.J. and Y.T. contributed to the animal experiments. All authors have given approval to the final version of the manuscript.

Notes

The authors declare no competing financial interest.

■ ACKNOWLEDGMENTS

This research was funded by the projects from CAMS Innovation Fund for Medical Sciences (grant no. CAMS-2017-I2M-1-007); The First Hospital of Jilin University (grant no. 0404694001) and Jilin Provincial Science-technologic Department (grant no. YDZJ202301ZYTS443).

■ REFERENCES

(1) Visscher, D. O.; Lee, H.; Van Zuijlen, P. P. M.; Helder, M. N.; Atala, A.; Yoo, J. J.; Lee, S. J. A Photo-Crosslinkable Cartilage-Derived Extracellular Matrix Bioink for Auricular Cartilage Tissue Engineering. *Acta Biomater.* **2021**, *121*, 193−203.

(2) Song, X.; Zhang, P.; Luo, B.; Li, K.; Liu, Y.; Wang, S.; Wang, Q.; Huang, J.; Qin, X.; Zhang, Y.; Zhou, G.; Lei, D. Multi-Tissue Integrated Tissue-Engineered Trachea Regeneration Based on 3D Printed Bioelastomer Scaffolds. *Advanced Science* **2024**, *11* (39), 2405420.

(3) Pang, L.; Jin, H.; Lu, Z.; Xie, F.; Shen, H.; Li, X.; Zhang, X.; Jiang, X.; Wu, L.; Zhang, M.; Zhang, T.; Zhai, Y.; Zhang, Y.; Guan, H.; Su, J.; Li, M.; Gao, J. Treatment with Mesenchymal Stem Cell-Derived Nanovesicle-Containing Gelatin Methacryloyl Hydrogels

Alleviates Osteoarthritis by Modulating Chondrogenesis and Macrophage Polarization. *Adv. Healthcare Mater.* **2023**, *12* (17), 2300315.
(4) Browe, D. C.; Mahon, O. R.; Díaz-Payno, P. J.; Cassidy, N.; Dudurych, I.; Dunne, A.; Buckley, C. T.; Kelly, D. J. Glyoxal Crosslinking of Solubilized Extracellular Matrix to Produce Highly Porous, Elastic, and Chondro-permissive Scaffolds for Orthopedic Tissue Engineering. *J. Biomed. Mater. Res* **2019**, *107* (10), 2222−2234.
(5) Feng, B.; Ji, T.; Wang, X.; Fu, W.; Ye, L.; Zhang, H.; Li, F. Engineering Cartilage Tissue Based on Cartilage-Derived Extracellular Matrix cECM/PCL Hybrid Nanofibrous Scaffold. *Mater. Des.* **2020**, *193*, 108773.
(6) Haghwerdi, F.; Ravari, M. K.; Taghiyar, L.; Shamekhi, M. A.; Jahangir, S.; Haririan, I.; Eslaminejad, M. B. Application of Bone and Cartilage Extracellular Matrices in Articular Cartilage Regeneration. *Biomed. Mater.* **2021**, *16* (4), 042014.
(7) Oh, H. J.; Kim, S. H.; Cho, J.-H.; Park, S.-H.; Min, B.-H. Mechanically Reinforced Extracellular Matrix Scaffold for Application of Cartilage Tissue Engineering. *Tissue Eng. Regen. Med.* **2018**, *15* (3), 287−299.
(8) Li, Y.; Liu, Y.; Xun, X.; Zhang, W.; Xu, Y.; Gu, D. Three-Dimensional Porous Scaffolds with Biomimetic Microarchitecture and Bioactivity for Cartilage Tissue Engineering. *ACS Appl. Mater. Interfaces* **2019**, *11* (40), 36359−36370.
(9) Sun, J.; Li, G.; Wu, S.; Zou, Y.; Weng, W.; Gai, T.; Chen, X.; Zhang, K.; Zhou, F.; Wang, X.; Su, J. Engineering Preparation and Sustained Delivery of Bone Functional Exosomes-Laden Biodegradable Hydrogel for in Situ Bone Regeneration. *Composites, Part B* **2023**, *261*, 110803.
(10) Tosoratti, E.; Fisch, P.; Taylor, S.; Laurent-Applegate, L. A.; Zenobi-Wong, M. 3D-Printed Reinforcement Scaffolds with Targeted Biodegradation Properties for the Tissue Engineering of Articular Cartilage. *Adv. Healthcare Mater.* **2021**, *10* (23), 2101094.
(11) Joyce, M.; Hodgkinson, T.; Lemoine, M.; González-Vázquez, A.; Kelly, D.; O'Brien, F. Development of a 3D-Printed Bioabsorbable Composite Scaffold with Mechanical Properties Suitable for Treating Large, Load-Bearingarticular Cartilage Defects. *eCM* **2023**, *45*, 158−172.
(12) Yang, Z.; Yi, P.; Liu, Z.; Zhang, W.; Mei, L.; Feng, C.; Tu, C.; Li, Z. Stem Cell-Laden Hydrogel-Based 3D Bioprinting for Bone and Cartilage Tissue Engineering. *Front. Bioeng. Biotechnol.* **2022**, *10*, 865770.
(13) Qin, Z.; Pang, Y.; Lu, C.; Yang, Y.; Gao, M.; Zheng, L.; Zhao, J. Photo-Crosslinkable Methacrylated Konjac Glucomannan (KGMMA) Hydrogels as a Promising Bioink for 3D Bioprinting. *Biomater. Sci.* **2022**, *10* (22), 6549−6557.
(14) Park, K. M.; Shin, Y. M.; Kim, K.; Shin, H. Tissue Engineering and Regenerative Medicine 2017: A Year in Review. *Tissue Eng. B Rev.* **2018**, *24* (5), 327−344.
(15) Iaquinta, M. R.; Mazzoni, E.; Manfrini, M.; D'Agostino, A.; Trevisiol, L.; Nocini, R.; Trombelli, L.; Barbanti-Brodano, G.; Martini, F.; Tognon, M. Innovative Biomaterials for Bone Regrowth. *Int. J. Mol. Sci.* **2019**, *20* (3), 618.
(16) Zhao, X.; Hua, Y.; Wang, T.; Ci, Z.; Zhang, Y.; Wang, X.; Lin, Q.; Zhu, L.; Zhou, G. In Vitro Cartilage Regeneration Regulated by a Hydrostatic Pressure Bioreactor Based on Hybrid Photocrosslinkable Hydrogels. *Front. Bioeng. Biotechnol.* **2022**, *10*, 916146.
(17) Lee, J. S.; Park, H. S.; Jung, H.; Lee, H.; Hong, H.; Lee, Y. J.; Suh, Y. J.; Lee, O. J.; Kim, S. H.; Park, C. H. 3D-Printable Photocurable Bioink for Cartilage Regeneration of Tonsil-Derived Mesenchymal Stem Cells. *Addit. Manuf.* **2020**, *33*, 101136.
(18) Behan, K.; Dufour, A.; Garcia, O.; Kelly, D. Methacrylated Cartilage ECM-Based Hydrogels as Injectables and Bioinks for Cartilage Tissue Engineering. *Biomolecules* **2022**, *12* (2), 216.
(19) Luo, C.; Xie, R.; Zhang, J.; Liu, Y.; Li, Z.; Zhang, Y.; Zhang, X.; Yuan, T.; Chen, Y.; Fan, W. Low-Temperature Three-Dimensional Printing of Tissue Cartilage Engineered with Gelatin Methacrylamide. *Tissue Eng. C Methods* **2020**, *26* (6), 306−316.
(20) Zhu, W.; Cui, H.; Boualam, B.; Masood, F.; Flynn, E.; Rao, R. D.; Zhang, Z.-Y.; Zhang, L. G. 3D Bioprinting Mesenchymal Stem Cell-Laden Construct with Core−Shell Nanospheres for Cartilage Tissue Engineering. *Nanotechnology* **2018**, *29* (18), 185101.
(21) Spencer, A. R.; Sani, E. S.; Soucy, J. R.; Corbet, C. C.; Primbetova, A.; Koppes, R. A.; Annabi, N. Bioprinting of a Cell-Laden Conductive Hydrogel Composite. *ACS Appl. Mater. Interfaces* **2019**, *11* (34), 30518−30533.
(22) Levato, R.; Lim, K. S.; Li, W.; Asua, A. U.; Peña, L. B.; Wang, M.; Falandt, M.; Bernal, P. N.; Gawlitta, D.; Zhang, Y. S.; Woodfield, T. B. F.; Malda, J. High-Resolution Lithographic Biofabrication of Hydrogels with Complex Microchannels from Low-Temperature-Soluble Gelatin Bioresins. *Mater. Today Bio* **2021**, *12*, 100162.
(23) Wang, Z.; Tian, Z.; Menard, F.; Kim, K. Comparative Study of Gelatin Methacrylate Hydrogels from Different Sources for Biofabrication Applications. *Biofabrication* **2017**, *9* (4), 044101.
(24) Ma, C.; Choi, J.-B.; Jang, Y.-S.; Kim, S.-Y.; Bae, T.-S.; Kim, Y.-K.; Park, J.-M.; Lee, M.-H. Mammalian and Fish Gelatin Methacryloyl−Alginate Interpenetrating Polymer Network Hydrogels for Tissue Engineering. *ACS Omega* **2021**, *6* (27), 17433−17441.
(25) Elkhoury, K.; Morsink, M.; Tahri, Y.; Kahn, C.; Cleymand, F.; Shin, S. R.; Arab-Tehrany, E.; Sanchez-Gonzalez, L. Synthesis and Characterization of C2C12-Laden Gelatin Methacryloyl (GelMA) from Marine and Mammalian Sources. *Int. J. Biol. Macromol.* **2021**, *183*, 918−926.
(26) Mishra, J.; Swain, J.; Mishra, A. K. Molecular Level Understanding of Sodium Dodecyl Sulfate (SDS) Induced Sol−Gel Transition of Pluronic F127 Using Fisetin as a Fluorescent Molecular Probe. *J. Phys. Chem. B* **2018**, *122* (1), 181−193.
(27) Ganguly, R.; Kumar, S.; Tripathi, A.; Basu, M.; Verma, G.; Sarma, H. D.; Chaudhari, D. P.; Aswal, V. K.; Melo, J. S. Structural and Therapeutic Properties of Pluronic® P123/F127 Micellar Systems and Their Modulation by Salt and Essential Oil. *J. Mol. Liq.* **2020**, *310*, 113231.
(28) Hopkins, C. C.; De Bruyn, J. R. Gelation and Long-Time Relaxation of Aqueous Solutions of Pluronic F127. *J. Rheol.* **2019**, *63* (1), 191−201.
(29) Li, P.; Zhang, C.; Li, R.; Qu, L.; Dai, X.; Sui, Y.; Hou, J. Multiple Physically Cross-Linked F127−α-CD Hydrogels: Preparation, Sol−Gel Transformation, and Controlled Release of 5-Fluorouracil. *ACS Appl. Bio Mater.* **2019**, *2* (1), 527−532.
(30) Albano, J.; Grillo, D.; Facelli, J.; Ferraro, M.; Pickholz, M. Study of the Lamellar and Micellar Phases of Pluronic F127: A Molecular Dynamics Approach. *Processes* **2019**, *7* (9), 606.
(31) Ren, P.; Zhang, H.; Dai, Z.; Ren, F.; Wu, Y.; Hou, R.; Zhu, Y.; Fu, J. Stiff Micelle-Crosslinked Hyaluronate Hydrogels with Low Swelling for Potential Cartilage Repair. *J. Mater. Chem. B* **2019**, *7* (36), 5490−5501.
(32) Gan, D.; Xu, T.; Xing, W.; Wang, M.; Fang, J.; Wang, K.; Ge, X.; Chan, C. W.; Ren, F.; Tan, H.; Lu, X. Mussel-Inspired Dopamine Oligomer Intercalated Tough and Resilient Gelatin Methacryloyl (GelMA) Hydrogels for Cartilage Regeneration. *J. Mater. Chem. B* **2019**, *7* (10), 1716−1725.
(33) Zhang, H.; Ren, P.; Jin, Y.; Ren, F. Injectable, Strongly Compressible Hyaluronic Acid Hydrogels via Incorporation of Pluronic F127 Diacrylate Nanomicelles. *Mater. Lett.* **2019**, *243*, 112−115.
(34) Chiesa-Estomba, C. M.; Hernáez-Moya, R.; Rodiño, C.; Delgado, A.; Fernández-Blanco, G.; Aldazabal, J.; Paredes, J.; Izeta, A.; Aiastui, A. Ex Vivo Maturation of 3D-Printed, Chondrocyte-Laden, Polycaprolactone-Based Scaffolds Prior to Transplantation Improves Engineered Cartilage Substitute Properties and Integration. *Cartil.* **2022**, *13* (4), 105−118.
(35) Kilmer, C. E.; Battistoni, C. M.; Cox, A.; Breur, G. J.; Panitch, A.; Liu, J. C. Collagen Type I and II Blend Hydrogel with Autologous Mesenchymal Stem Cells as a Scaffold for Articular Cartilage Defect Repair. *ACS Biomater. Sci. Eng.* **2020**, *6* (6), 3464−3476.
(36) Grenier, J.; Duval, H.; Barou, F.; Lv, P.; David, B.; Letourneur, D. Mechanisms of Pore Formation in Hydrogel Scaffolds Textured by Freeze-Drying. *Acta Biomater.* **2019**, *94*, 195−203.

https://doi.org/10.1021/acsomega.5c00476
ACS Omega 2025, 10, 13570−13582

(37) Krishnamoorthy, S.; Noorani, B.; Xu, C. Effects of Encapsulated Cells on the Physical−Mechanical Properties and Microstructure of Gelatin Methacrylate Hydrogels. *Int. J. Mol. Sci.* **2019**, *20* (20), 5061.
(38) Lutzweiler, G.; Barthes, J.; Koenig, G.; Kerdjoudj, H.; Mayingi, J.; Boulmedais, F.; Schaaf, P.; Drenckhan, W.; Vrana, N. E. Modulation of Cellular Colonization of Porous Polyurethane Scaffolds via the Control of Pore Interconnection Size and Nanoscale Surface Modifications. *ACS Appl. Mater. Interfaces* **2019**, *11* (22), 19819−19829.
(39) Han, Y.; Lian, M.; Wu, Q.; Qiao, Z.; Sun, B.; Dai, K. Effect of Pore Size on Cell Behavior Using Melt Electrowritten Scaffolds. *Front. Bioeng. Biotechnol.* **2021**, *9*, 629270.
(40) Buenzli, P. R.; Lanaro, M.; Wong, C. S.; McLaughlin, M. P.; Allenby, M. C.; Woodruff, M. A.; Simpson, M. J. Cell Proliferation and Migration Explain Pore Bridging Dynamics in 3D Printed Scaffolds of Different Pore Size. *Acta Biomater.* **2020**, *114*, 285−295.
(41) Lu, D.; Zeng, Z.; Geng, Z.; Guo, C.; Pei, D.; Zhang, J.; Yu, S. Macroporous Methacrylated Hyaluronic Acid Hydrogel with Different Pore Sizes for in Vitro and in Vivo Evaluation of Vascularization. *Biomed. Mater.* **2022**, *17* (2), 025006.
(42) Zhou, L.; Pei, X.; Fang, K.; Zhang, R.; Fu, J. Super Tough, Ultra-Stretchable, and Fast Recoverable Double Network Hydrogels Physically Crosslinked by Triple Non-Covalent Interactions. *Polymer* **2020**, *192*, 122319.
(43) Chen, N.; Zhu, K.; Zhang, Y. S.; Yan, S.; Pan, T.; Abudupataer, M.; Yu, G.; Alam, Md. F.; Wang, L.; Sun, X.; Yu, Y.; Wang, C.; Zhang, W. Hydrogel Bioink with Multilayered Interfaces Improves Dispersibility of Encapsulated Cells in Extrusion Bioprinting. *ACS Appl. Mater. Interfaces* **2019**, *11* (34), 30585−30595.
(44) Piantanida, E.; Alonci, G.; Bertucci, A.; De Cola, L. Design of Nanocomposite Injectable Hydrogels for Minimally Invasive Surgery. *Acc. Chem. Res.* **2019**, *52* (8), 2101−2112.
(45) Townsend, J. M.; Beck, E. C.; Gehrke, S. H.; Berkland, C. J.; Detamore, M. S. Flow Behavior Prior to Crosslinking: The Need for Precursor Rheology for Placement of Hydrogels in Medical Applications and for 3D Bioprinting. *Prog. Polym. Sci.* **2019**, *91*, 126−140.
(46) Zhan, Y.; Fu, W.; Xing, Y.; Ma, X.; Chen, C. Advances in Versatile Anti-Swelling Polymer Hydrogels. *Mater. Sci. Eng. C* **2021**, *127*, 112208.
(47) Zhao, D.; Wang, X.; Cheng, B.; Yin, M.; Hou, Z.; Li, X.; Liu, K.; Tie, C.; Yin, M. Degradation-Kinetics-Controllable and Tissue-Regeneration-Matchable Photocross-Linked Alginate Hydrogels for Bone Repair. *ACS Appl. Mater. Interfaces* **2022**, *14* (19), 21886−21905.
(48) Gao, J.; Li, M.; Cheng, J.; Liu, X.; Liu, Z.; Liu, J.; Tang, P. 3D-Printed GelMA/PEGDA/F127DA Scaffolds for Bone Regeneration. *J. Funct. Biomater.* **2023**, *14* (2), 96.
(49) Gu, L.; Li, T.; Song, X.; Yang, X.; Li, S.; Chen, L.; Liu, P.; Gong, X.; Chen, C.; Sun, L. Preparation and Characterization of Methacrylated Gelatin/Bacterial Cellulose Composite Hydrogels for Cartilage Tissue Engineering. *Regener. Biomater.* **2020**, *7* (2), 195−202.
(50) Aldana, A. A.; Valente, F.; Dilley, R.; Doyle, B. Development of 3D Bioprinted GelMA-Alginate Hydrogels with Tunable Mechanical Properties. *Bioprinting* **2021**, *21*, No. e00105.
(51) Yi, X.; He, J.; Wang, X.; Zhang, Y.; Tan, G.; Zhou, Z.; Chen, J.; Chen, D.; Wang, R.; Tian, W.; Yu, P.; Zhou, L.; Ning, C. Tunable Mechanical, Antibacterial, and Cytocompatible Hydrogels Based on a Functionalized Dual Network of Metal Coordination Bonds and Covalent Crosslinking. *ACS Appl. Mater. Interfaces* **2018**, *10* (7), 6190−6198.
(52) Li, X.; Sheng, S.; Li, G.; Hu, Y.; Zhou, F.; Geng, Z.; Su, J. Research Progress in Hydrogels for Cartilage Organoids. *Adv. Healthcare Mater.* **2024**, *13* (22), 2400431.
(53) Shen, C.; Zhou, Z.; Li, R.; Yang, S.; Zhou, D.; Zhou, F.; Geng, Z.; Su, J. Silk Fibroin-Based Hydrogels for Cartilage Organoids in Osteoarthritis Treatment. *Theranostics* **2025**, *15* (2), 560−584.
(54) Wei, J.; Baptista-Hon, D. T.; Wang, Z.; Li, G.; Herrler, T.; Dai, C.; Liu, K.; Yu, B.; Chen, X.; Yang, M.; Han, D.; Gao, Y.; Huang, R.-L.; Guo, L.; Zhang, K.; Li, Q. Bioengineered Human Tissue Regeneration and Repair Using Endogenous Stem Cells. *Cell Rep. Med.* **2023**, *4* (8), 101156.
(55) Sahranavard, M.; Sarkari, S.; Safavi, S.; Ghorbani, F. Three-Dimensional Bio-Printing of Decellularized Extracellular Matrix-Based Bio-Inks for Cartilage Regeneration: A Systematic Review. *Biomater. Transl.* **2022**, *3* (2), 105−115.

https://doi.org/10.1021/acsomega.5c00476
ACS Omega 2025, 10, 13570−13582